Chapter 9

Gas Permeability Behavior of Porous Alumina Developed using Rice Husk and Sucrose

9.1. Introduction

Porous ceramics find wide range of technological applications in gas/liquid separator, low as well as high temperature fluid filters, catalyst carriers, heat exchangers, thermal insulations, solid oxide fuel cells, high efficiency combustion burners, biomedical implants etc.,[103-109,182] as a result of their distinct properties such as low bulk density, high porosity, high specific surface area, low thermal conductivity, high temperature resistance, high thermal shock resistance, low thermal mass, high specific strength etc. Furthermore, porous ceramics have become ideal substitutes for conventional porous media in many fields of science and engineering because they offer some advantages over beds of packed particles.[183] In the past few years, applications of porous ceramics as filters have generated considerable interest in various technological applications like metal refinement, diesel combustion, hot gas filtration, residues burning etc,[184-186] due to their thermal resistance at high temperatures (usually > 1000˚C). In high temperature gas filtration (usually in the range of 300˚C-900˚C), the gas flows through porous ceramic filters designed to satisfy the stringent environmental laws in the control of particulate emission.

According to their structures and constituents, hot gas ceramic filters can be divided into two main categories: granular and fibrous filters. Ideally, the ceramic filter should be able to remove the maximum of impurities with minimum resistance to the flow of fluids. One of the most important properties of porous ceramics employed in filtration applications is permeability.[187] Higher permeability is thought to be obtained by controlling the porosity and pore microstructure such as pore size, pore shape, and extent of pore connectivity of porous ceramics.[25,188-190] Also, higher porosity though increase the permeability, reduce the mechanical properties.[191-198]

Therefore, optimization between permeability and mechanical strength of porous ceramics is a basic requirement for adequate operation of the ceramic as a filter material. This depends on the ideal combination of pore size and porosity.[130] Permeability and mechanical strength are distinctly affected for a determined porous structure. Large pores favor the permeability but reduce the collection efficiency of particles. On the other hand, small pores increase the efficiency and increase the pressure drop through the filter.[184] Additionally, in gas filtration, the fractional collection efficiency is also sensitive to the nominal pore count and tortuosity of the structural layer.[184,199] Approach to satisfy both properties is best realized through increase in extent of pore interconnection during processing.[130]

Fabrication of porous ceramics with tailored permeability and mechanical properties via various techniques have found an increasing demand in various solid-fluid separation processes, such as filters. Various researchers have reported fabrication of porous compacts with range of permeability. Isobe et al.[130] prepared porous alumina ceramics with unidirectionally aligned cylindrical pores by an extrusion method using fibers with a diameter of 43 μm as pore forming agent and the permeability of the resulted sample having 39% porosity was $3.9x10^{-3}$ m^2. Yang et al.[189] fabricated porous cordierite ceramics with well distributed interconnected pores through a pore-forming in-situ technique and the permeability of the sample with a porosity of 40.3% and an average pore size of 23.3 μm was $2.31x10^{-12}$ m^2. A comparison of the permeability of the samples having above mentioned two pore structures, it seems that those with a well distributed interconnected pores has a comparatively higher gas permeability. Additionally, the porosity, pore size, distribution of pores, pore shape also affects the strength of porous ceramics. A smaller pore size and a homogeneous pore distribution are generally helpful to improve the strength of porous ceramics. In this connection, porous ceramics fabricated through the pore forming in-situ technique have a high strength due to their small pore size and well-distributed interconnected pores depending on the composition and microstructure.[200]

Although, in all fabrication routes, the final shapes display a large porosity level, the general pore microstructure and corresponding mechanical properties of

porous ceramics are different in each case. Each method has its own advantages and potential uses. The control of processing steps and consequently, the ultimate material properties in terms of pore microstructure is a common requirement for all fabrication processes.

From the view point of producing cost effective porous ceramics having wide range of interconnected pore microstructure as well as adequate strength and considering the increasing demand of potential use of porous ceramics in filtration applications in various technological fields, attempts were made to characterize the permeability behavior of the developed porous alumina and correlate the results with the microstructure of the developed porous alumina. The influence of porosity and pore size on the measured permeability and strength has been examined. Also, the variations of flow rate with the pressure drop for different compositions have been highlighted. The experimental results of permeability were compared with the predicted values obtained using Forchheimer's equation.

In the present study, porous alumina ceramics specifically with randomly oriented interconnected pores have been chosen for permeability measurement. The observed permeability and strength results were co-related with the volume fraction porosity and pore size of samples in order to establish a desirable compositions and processing parameters for the selection of porous ceramics in applications where a high degree of permeability along with adequate mechanical strength is required.

9.2. Theory

The permeability of a porous medium at room temperature can be well described by Forchhemier's equation (Eqn. 9.2),[110,201] which displays a parabolic trend of the pressure drop with the superficial fluid velocity (v_s). Permeability of a material relates to the pressure drop that is developed across the thickness of the material as a fluid flows through it. Higher permeability materials would result in lower pressure drops across the thickness for a certain flow rate. An ASTM standard (C577– 99) has defined the method for measuring permeability of porous refractory materials. The interaction between fluid and the porous medium that results in fluid pressure drop varies with fluid flow velocity. For low fluid

velocity (R_e= ($\rho v_s/\mu$)*(k_1/k_2) << 1), the equation proposed by Darcy (1856), originally proposed for packed granular beads, can be used for calculating the permeability of a porous medium.

$$\frac{\Delta P}{L} = \left(\frac{\mu}{k_1}\right) \times v_S \quad \text{.....(9.1)}$$

where ΔP= pressure drop, L= thickness of the sample (parallel to the fluid flow), μ= Dynamic fluid viscosity, k_1= Darcian permeability and v_s= fluid velocity

The Darcy's equation accounts for only the viscous effects of the fluid. The above equation was modified by Reynolds (1900) and Forchheimer (1901) to include both the viscous and inertial effects

$$\frac{\Delta P}{L} = \left(\frac{\mu}{k_1}\right) \times v_S + \left(\frac{\rho}{k_2}\right) \times v_S{}^2 \quad \text{.....(9.2)}$$

where ρ is the density of fluid, k_2= non-Darcian permeability, $\Delta P = P_i - P_o$ for liquids and $\Delta P = P_i^2 - P_o^2/2Po$ for gases. P_i and P_o are pressure values at the entrance and exit respectively.

Both permeabilities depend exclusively on the porous structure.[190] The first term of the right side of Eqn. 9.1 represents a linear term which expresses the contribution of the attrition effects to flow resistance (viscous regime) and the latter part represents a quadratic term which describes the contribution of kinetic effects on the pressure drop inertial force (turbulent regime). Both k_1 and k_2 have a non-linear dependence on the porosity and pore size.

Ergun[202] in 1952 defined the permeability constants (k_1, k_2) directly in terms of the flow through granular packed bed as:

$$k_1 = \frac{\varepsilon^3 d_p{}^2}{150\ (1-\varepsilon)^2} \quad \text{.....(9.3)}$$

$$k_2 = \frac{\varepsilon^3 {d_p}^2}{1.75(1-\varepsilon)} \quad \text{.....(9.4)}$$

where ε is the bed porosity and d_p is the mean particle diameter of the granular medium. These equations have been applied in consolidated materials with configured cell (pore) structures such as porous ceramics, where the particle diameter (d_p) in Eqn. 9.3 and Eqn. 9.4 has been replaced with average pore size by some researchers.[202] As per the above equations, Both Darcian (k_1) and non-Darcian permeability (k_2) have a non-linear dependeceon the porosity and pore size. When the kinetic effects are negligible, Eqn. 9.2 reduces to Darcy's law which displays only the linear dependence of the gas velocity on the pressure gradient. Commercial ceramic filters exhibit Darcian permeability typically in the range of 10^{-10}-10^{-8} m^2 and compressive strength varying from 0.5 to 2 MPa.[185]

9.3. Sample Preparation and Characterization

The procedure for sample preparation has already been mentioned in detail in chapter 5. The gas permeability was measured under nitrogen gas flow in a permeability set up, which is shown in Fig. 9.1 The actual set up is shown in Fig. 9.2.

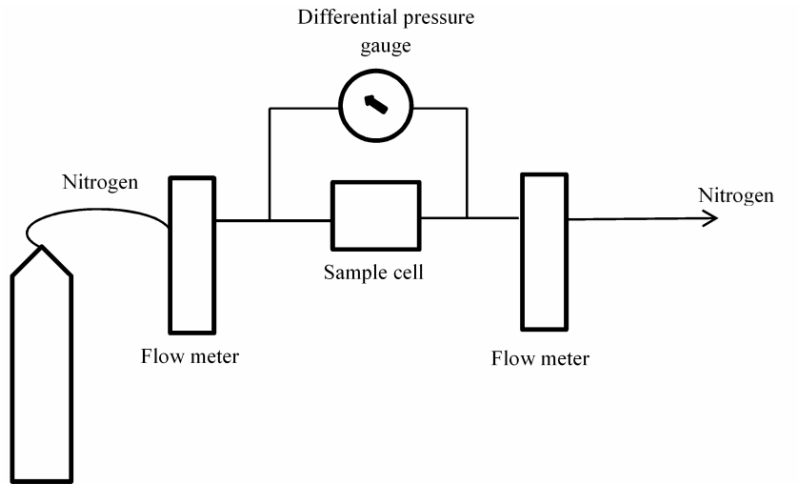

Fig. 9.1 Schematic of the set-up used for measuring gas permeability.

Fig. 9.2 Set up for measurement of gas permeability of porous ceramics

For the above measurements, rectangular samples with dimensions 15 mm x 15 mm x 15 mm (thickness) were sealed in a rubber gasket inside the metallic sample holder. Then nitrogen gas was allowed to flow through the porous sample. The inlet pressure of the flow of nitrogen gas was maintained at 4 bar and the flow rates were controlled in the range of 2 liters per minute (LPM) to 210 LPM using a calibrated mass flow meter. For each flow rate, the pressure drop across the porous sample was measured using a differential pressure gauge.

The permeability[185,202-203] was calculated using the Eqn. 9.2 given in theory section. μ is the dynamic viscosity of nitrogen (in this work, μ= 1.75x10^{-5} Pa.s at 25˚C and ρ is the density of nitrogen (1.13 Kg/m^3 at 25˚C), v_s is the gas velocity, k_1 & k_2 are Darcian and non-Darcian permeability constants respectively. The list of samples with their compositions used for permeability measurement is given in Table 9.1.

Table 9.1 List of selected sample compositions (wt% basis) for permeability measurement

$Al\_^{x}RH_{y}\_SS_{20}$					
RH size (µm)	RH content (wt%)				
	20	25	30	35	40
< 75	$Al\_^{<75}RH_{20}\_SS_{20}$	$Al\_^{<75}RH_{25}\_SS_{20}$	$Al\_^{<75}RH_{30}\_SS_{20}$	$Al\_^{<75}RH_{35}\_SS_{20}$	$Al\_^{<75}RH_{40}\_SS_{20}$
75-180	$Al\_^{75\text{-}180}RH_{20}\_SS_{20}$	$Al\_^{75\text{-}180}RH_{25}\_SS_{20}$	$Al\_^{75\text{-}180}RH_{30}\_SS_{20}$	$Al\_^{75\text{-}180}RH_{35}\_SS_{20}$	$Al\_^{75\text{-}180}RH_{40}\_SS_{20}$
180-355	$Al\_^{180\text{-}355}RH_{20}\_SS_{20}$	$Al\_^{180\text{-}355}RH_{25}\_SS_{20}$	$Al\_^{180\text{-}355}RH_{30}\_SS_{20}$	$Al\_^{180\text{-}355}RH_{35}\_SS_{20}$	$Al\_^{180\text{-}355}RH_{40}\_SS_{20}$
355-420	$Al\_^{355\text{-}420}RH_{20}\_SS_{20}$	$Al\_^{355\text{-}420}RH_{25}\_SS_{20}$	$Al\_^{355\text{-}420}RH_{30}\_SS_{20}$	$Al\_^{355\text{-}420}RH_{35}\_SS_{20}$	$Al\_^{355\text{-}420}RH_{40}\_SS_{20}$
420-600	$Al\_^{420\text{-}600}RH_{20}\_SS_{20}$	$Al\_^{420\text{-}600}RH_{25}\_SS_{20}$	$\#\ Al\_^{420\text{-}600}RH_{30}\_SS_{20}$	$\#Al\_^{420\text{-}600}RH_{35}\_SS_{20}$	$\#\ Al\_^{420\text{-}600}RH_{40}\_SS_{20}$

9.4. Results and Discussion

Permeability experiments were performed with nitrogen gas at room temperature. Fig. 9.3 shows the permeability curves (pressure drop versus nitrogen gas flow) of the RH based porous alumina samples derived from

different compositions. It was seen that the resistance to flow of the samples significantly differ for different compositions and exhibit the parabolic trend proposed by Forchheimer (Eqn. 9.2) rather than the linear relationship between pressure drop and fluid velocity stated by Darcy's law.

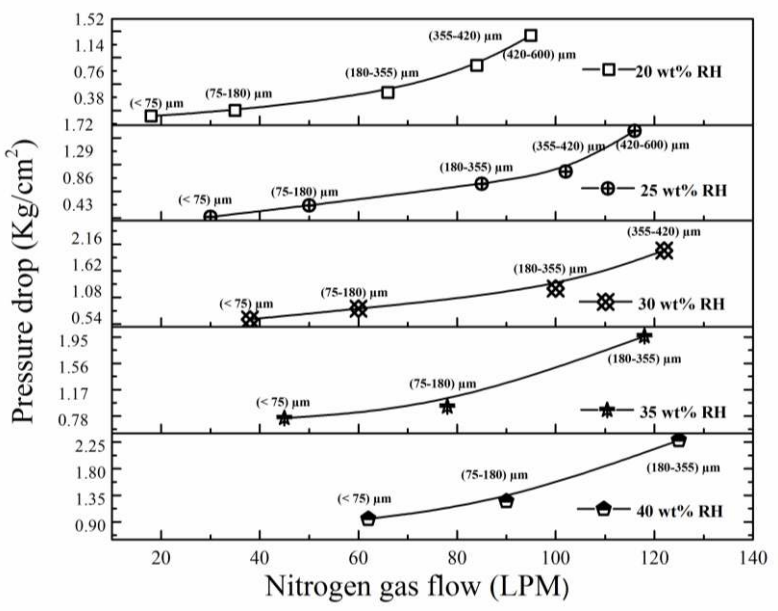

Fig. 9.3 Variation of pressure drop with nitrogen gas flow at fixed pressure across porous alumina compacts

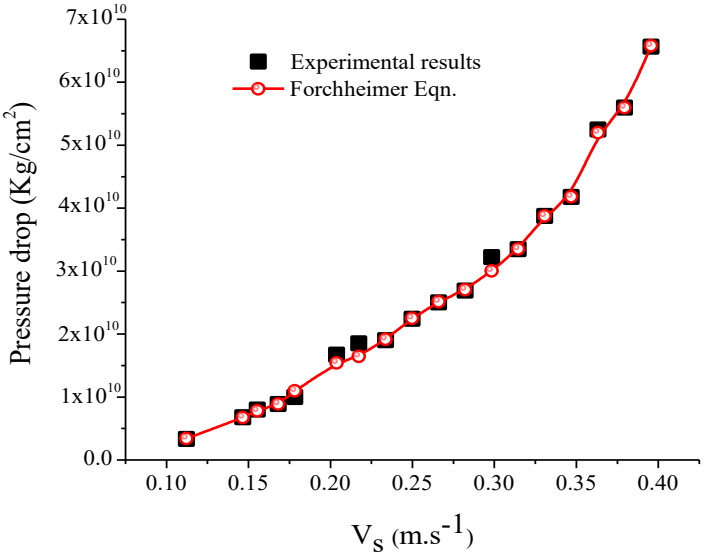

Fig. 9.4 Pressure drop as a function of flow rate for predicted results and experimental results

The intensity of the quadratic term increases at a faster rate for velocities higher than 0.2 m/s (approximately), suggesting very low values for inertial non-Darcian permeability term in the analysis (Fig. 9.4).

Also, the pressure drop as a function of flow rate appeared to co-relate well with the expectation as per the microstructural features. For the same nitrogen flow rate, it was seen that the porous alumina samples prepared with higher RH content which yielded higher porosity caused the lowest pressure drop of nitrogen through the sample. For similar reasons, porous alumina samples prepared with the same RH content in the composition, the pressure drop at a fixed flow rate was higher for samples with coarser size RH powder (Fig. 9.5). The nitrogen flow rate through the porous alumina, for any fixed pressure drop, decreased with increase in RH size for sample prepared from a fixed RH content (Fig. 9.5). The flow rate was highest for the sample prepared with 40 wt% RH and lowest for those prepared with 20 wt% RH (Fig. 9.5). The flow rate increased with increase in total porosity of the sample. This can be attributed to the increase in the extent of interconnection between pores in the porous ceramics leading to increase in flow rate.

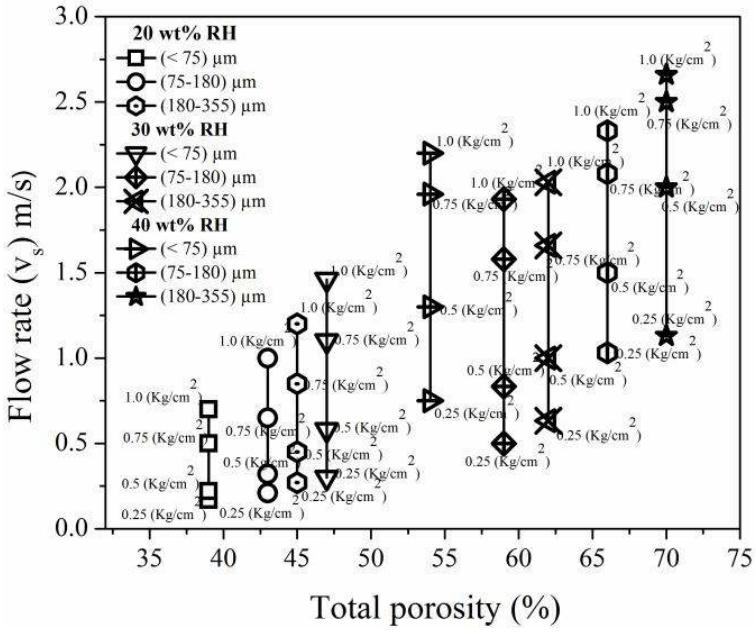

Fig. 9.5 Variation of flow rate with total porosity for various nitrogen gas at different pressure across porous alumina compacts

The gas permeability behavior of porous alumina in terms of variation in permeability constants, Darcian (k_1) and non-Darcian (k_2), as a function of volume fraction porosity and pore size, respectively is shown in Fig. 9.6 and Fig. 9.7. The values of k_1 and k_2 against each composition is displayesd in Table 9.2.

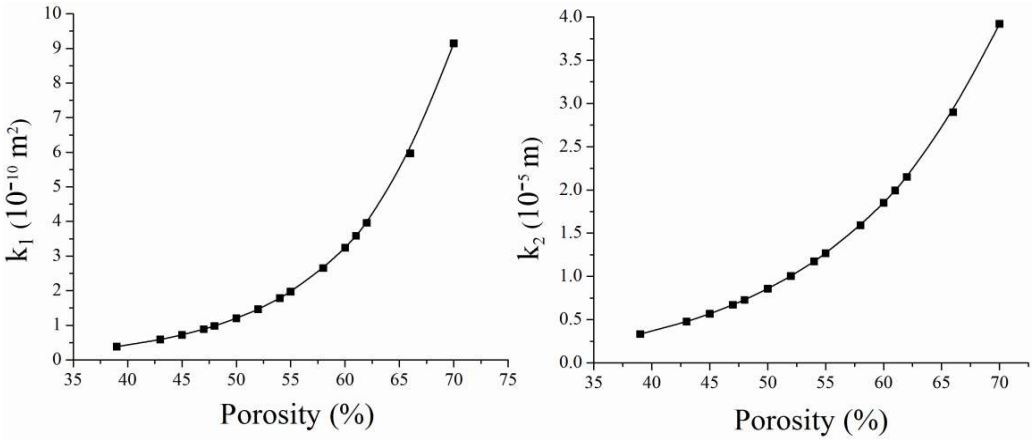

Fig. 9.6 Variation of (a) Darcian permeability k_1 and (b) non-Darcian permeability k_2 with porosity of porous alumina compacts.

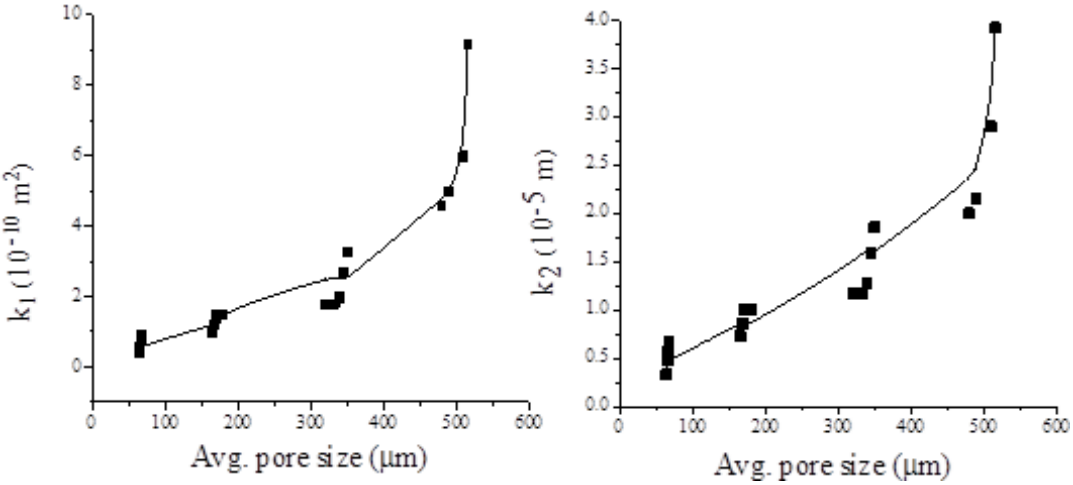

Fig. 9.7 Variation of (a) Darcian permeability k_1 and (b) non-Darcian permeability k_2 with pore size of porous alumina compacts

Table 9.2 Variation of (a) Darcian permeability k_1 and (b) non-Darcian permeability k_2 with pore size of porous alumina compacts

Al_^{x}RH$_y$_SS$_{20}$		Porosity (vol %)	Avg. Pore Size (μm)	Isolated/ interconnected	Three point bending strength	K_1 x 10^{-10}	K_2 x 10^{-5}	Compressive strength
RH Content (wt %)	RH size(μm)							
20	< 75	39	65.15	64	98	0.3826	0.33341	82
	75-180	43	60.8	165.7	89	0.58731	0.47824	65
	180-355	45	56.0	320.5	58.1	0.58731	0.47824	48
	355-420	54	53	480	40	0.72298	0.56805	31
	420-600	61	45.45	510	28	0.88706	0.67163	20.13
25	< 75	43	59	65	88	0.98159	0.72918	58
	75-180	48	56	168.5	65	1.2	0.85714	45
	180-355	50	52	333	45	1.46467	1.00434	34
	355-420	58	50	490	36	1.46467	1.00434	28
	420-600	64	42.2	516	34	1.46467	1.00434	18
30	< 75	47	53.0	66	48	1.78598	1.17364	33
	75-180	52	50.5	170	32	1.78598	1.17364	23
	180-355	60	49.2	340	24	1.97185	1.26762	14.67
	355-420	65	48.32	498	20	2.2178	1.38268	8.67
35	< 75	52	50	67	42	2.65459	1.59275	26
	75-180	58	48	175	30	3.24	1.85143	18
	180-355	62	46	345	27	3.58155	1.99544	7
40	< 75	54	47.97	68	42	3.96113	2.15033	22.24
	75-180	66	46.6	180	22	5.96878	2.89912	9.18
	180-355	70	44.1	350	14	9.14667	3.92	6

It appears from the figures that they obey the Forchhemier's equation. Permeability was observed for all samples, even with the sample Al_$^{<75}$RH$_{20}$_SS$_{20}$ having minimum porosity of 39 vol% and smallest avg. pore size of 64 μm. This observation is in good agreement with the calculated percolation limit of porosity of >31% from the percolation model.[204] Also, as expected, both the Darcian and non-Darcian permeability increased with increase

in porosity and pore size of porous samples. It is interesting to note that, the increase in permeability (both k_1 and k_2) of samples with porosity (Fig. 9.6 (a) and Fig. 9.6 (b)) was initially slow and within a narrow range up to a porosity of approximately 55 vol %, beyond which a rapid increase in permeability was observed. Similarly, a slow increase in both Darcian (k_1) and non-Darcian (k_2) permeability was observed for samples with pore size up to approximately 500 μm and above that permeability increased at a very fast rate. Similar observation on the dependence of permeability on porosity, pore size was reported by Salvini et al. and Innocentiniet al.[202]

The increase in permeability is attributed to the increase of the fluid-solid contact area caused by the increase in porosity and pore size. Also, the main path for gas transport gradually increases as the pores join together resulting in more connectivity (extent of interconnection) of pores with increase in porosity and pore size of porous samples (shown clearly in micrographs). It can be seen that the porous samples with the maximum porosity showed the maximum value of Darcian permeability. The measured Darcian and non Darcian permeability was in the range 0.383-9.14 $x10^{-10}$ m^2 and 0.33-3.92 $x10^{-7}$ m, respectively, for the developed porous alumina compacts. In comparison, for porous gelcast samples with nearly similar porosity (approximately 34 %) the Darcian and non Darcian permeability values have been reported to be around $5.1x10^{-11}$ m^2 and $6.19x10^{-6}$ m, respectively.[205] The observation of little lower Darcian permeability for RH based porous samples in comparison to the gel cast sample of comparable porosity is in accordance with comparatively lower extent of interconnections between pores in RH based porous samples, consequently less channels for gas flow.

The measured permeability constant (k_1) of a typical RH based sample ($Al\_^{<75}RH_{20}\_SS_{20}$) with porosity 39 vol% and avg. pore size of 64 μm was $0.383x10^{-10}$ m^2. In comparison, the permeability of extruded samples with unidirectionally aligned pores having 39% porosity has been reported to be $4.1x10^{-14}$ m^2 which is very less as compared to that of our samples.[130] Similarly, Darcian permeability of RH based porous alumina sample ($Al\_^{75\text{-}180}RH_{20}\_SS_{20}$)

having porosity of 43 vol% and avg. pore size of 165.7 µm was measured to be $0.587x10^{-10}$ m^2. The reported value of permeability of a conventional partially sintered porous sample having 43% porosity was $1.0x10^{-16}$ m^2,[130] which is comparatively low. Thus, the observed gas permeability values of RH based porous ceramics developed in the present process are better than those reported in the literature. Hence, by varying the RH content and its size in the composition, the porosity, pore size and the extent of pore interconnection of samples can be controlled which ultimately influences the permeability characteristics in a wide range. The variation of k_2 with porosity and pore size can be explained in terms of kinetic effects due to variation in microstructure in RH based porous alumina. Smaller pores and low porosity increase the flow resistance of the nitrogen gas.

Maximum Darcian permeability of $9.14x10^{-10}$ m^2 was observed for the sample $Al\_^{180\text{-}355}RH_{40}\_SS_{20}$ which showed minimum compressive strength of 6 MPa and the sample $Al\_^{<75}RH_{20}\_SS_{20}$ having maximum crushing strength of 82 MPa showed minimum permeability of $0.38x10^{-10}$ m^2. Based on the above results, an optimum combination between the two parameters such as permeability and strength can be made while choosing a sample for the selected application such as filtration in order to achieve best possible performance of the end product.

9.5. Summary

The pressure drop through the porous alumina within the tested range of nitrogen gas velocity is described by a parabolic behavior (Forchheimer' sequation), which was characterized by a Darcian permeability constant (k_1) and non-Darcian permeability constant (k_2), related to viscous and inertial fluid regimes, respectively.

1. The Darcian permeability of porous alumina was found to be in the range of 0.38-9.15 $x10^{-10}$ m^2, which of right the order of magnitude for gas filters, and therefore, suitable for various technological applications.
2. The non-Darcian permeability (k_2) was in the range of 0.33-3.92 $x10^{-5}$ m.
3. Experimental results fitted well with the theoretical predictions made using Forchhemier equation.

4. It was seen that, the gas permeability of the developed porous ceramics was strongly dependent on their porosity and pore size.
5. Minimum permeability was obtained for the sample $Al\_^{<75}RH_{20}\_SS_{20}$ which exhibited maximum strength. The sample $Al\_^{180\text{-}355}RH_{40}\_SS_{20}$ with maximum permeability exhibited minimum strength.
6. The results showed that the permeability of porous alumina varied several orders of magnitude according to the volume fraction and size of RH pore former, indicating the possibility of tailoring these two parameters such as RH content and its particle size according to the requirements of the specific application considered.
7. An increase in porosity and pore size of samples though resulted in a remarkable increase in gas permeability, decreased the mechanical properties
8. Thus, porous ceramics with high permeability and reasonable strength can be achieved through proper selection of the composition and the corresponding microstructure.